Optimized Reduced Chemistry and Molecular Transport for Large Eddy Simulation of Partially Premixed Combustion in a Gas Turbine

Article *in* Combustion Science and Technology · July 2015

DOI: 10.1080/00102202.2015.1074574

CITATIONS
25

READS
1,768

6 authors, including:

Abdallah Abou-Taouk
Azelio AB
20 PUBLICATIONS **154** CITATIONS
SEE PROFILE

Pascale Domingo
CORIA
147 PUBLICATIONS **4,332** CITATIONS
SEE PROFILE

Luc Vervisch
Institut National des Sciences Appliquées de Rouen
270 PUBLICATIONS **8,524** CITATIONS
SEE PROFILE

Taylor & Francis
Taylor & Francis Group

Combustion Science and Technology

ISSN: 0010-2202 (Print) 1563-521X (Online) Journal homepage: http://www.tandfonline.com/loi/gcst20

Optimized Reduced Chemistry and Molecular Transport for Large Eddy Simulation of Partially Premixed Combustion in a Gas Turbine

A. Abou-Taouk, B. Farcy, P. Domingo, L. Vervisch, S. Sadasivuni & L.-E. Eriksson

To cite this article: A. Abou-Taouk, B. Farcy, P. Domingo, L. Vervisch, S. Sadasivuni & L.-E. Eriksson (2016) Optimized Reduced Chemistry and Molecular Transport for Large Eddy Simulation of Partially Premixed Combustion in a Gas Turbine, Combustion Science and Technology, 188:1, 21-39, DOI: 10.1080/00102202.2015.1074574

To link to this article: http://dx.doi.org/10.1080/00102202.2015.1074574

COMBUSTION SCIENCE AND TECHNOLOGY
2016, VOL. 188, NO. 1, 21–39
http://dx.doi.org/10.1080/00102202.2015.1074574

Taylor & Francis
Taylor & Francis Group

Optimized Reduced Chemistry and Molecular Transport for Large Eddy Simulation of Partially Premixed Combustion in a Gas Turbine

A. Abou-Taouk[a], B. Farcy[b,c], P. Domingo[b], L. Vervisch[b], S. Sadasivuni[d], and L.-E. Eriksson[a]

[a]Chalmers University of Technology, Gothenburg, Sweden; [b]CORIA—CNRS & INSA Rouen, Normandie Université, Rouen, France; [c]SOLVAY Research & Innovation—Lyon Center, Lyon, France; [d]Siemens Industrial Turbomachinery Ltd, Waterside South, Lincoln, UK

ABSTRACT

A methodology is discussed to automatically determine the parameters of closed budget equations for chemical species mass fractions and energy, in order to simulate spatially filtered flames as required in large eddy simulation (LES). The method accounts for the effects of LES filtering on chemistry and transport by simultaneously optimizing, for a reduced number of species, the Arrhenius reaction rates and a correction to mixture-averaged molecular diffusion coefficients. The objective is to match, for a given filter size, spatially filtered canonical one-dimensional flames simulated with detailed chemistry solutions. This approach is designed for quite well-resolved LES, in which most of the unresolved fluctuations result from flame thickening due to spatial filtering, thus featuring weak levels of sub-grid scale flame wrinkling. Methane-air partially premixed combustion is addressed. A four-step reduced reaction mechanism involving seven species is developed along with mass and heat molecular transport properties. The optimization is performed at atmospheric pressure and at 3 bar, for ranges of fresh gas temperatures [300–650 K] and equivalence ratios [0.4–1.2]. Comparisons with the filtered detailed chemistry solution of a planar propagating front show that the laminar flame speed, the adiabatic flame temperature, the species profiles in the reaction zone, and the flow chemical composition and temperature at equilibrium are adequately predicted. The new sub-grid scale modeling approach is then applied to three-dimensional LES of an industrial gas turbine burner. Good agreement is found between the quantities predicted with LES and experimental data, in terms of flow and flame dynamics, axial velocities, averaged temperatures, and some major species concentrations. Results are also improved compared to previous simulations of the same burner.

ARTICLE HISTORY
Received 28 May 2015
Revised 8 July 2015
Accepted 16 July 2015

KEYWORDS
Chemistry reduction; flame filtering optimization; large eddy simulation; partially premixed turbulent flames; swirling flames

Introduction

The range of turbulent reacting flows to which large eddy simulation (LES) is applied is rapidly growing, from laboratory jet-flames (Nambully et al., 2014b; Proch and Kempf, 2014) up to full-size industrial burners (Gicquel et al., 2012; Lecocq et al., 2014; Srinivasan

CONTACT A. Abou-Taouk abdallah@chalmers.se Division of Fluid Dynamics, Department of Applied Mechanics, Chalmers University of Technology, SE-41296 Gothenburg, Sweden.

Color versions of one or more of the figures in the article can be found online at www.tandfonline.com/gcst.

et al., 2015). Within this numerical modeling framework, the largest flow scales are simulated over a mesh too coarse to resolve the smallest eddies. The dissipative character of these smallest scales is approximated through a modeled expression for an eddy viscosity (Ferziger, 1993; Moin, 2002; Sagaut, 2001). Formally, the flow resolved by the LES mesh is obtained from the solution of the aero-thermochemistry equations, to which a spatial filtering operation has been applied in order to remove fluctuations smaller than a characteristic filter length-scale (Lesieur et al., 2005).

The application of LES to real burner geometries and the corresponding subgrid scale modeling challenges have been the subject of numerous studies over the past 10 years (Boudier et al., 2008; Domingo and Vervisch, 2015; Fiorina et al., 2010; Gicquel et al., 2012; Marincola et al., 2013; Nambully et al., 2014a; Pitsch, 2006; Subramanian et al., 2010; Triantafyllidis et al., 2009). The problem is twofold. First, the complexity of combustion chemistry must be reduced to limit the number of degrees of freedom and the stiffness of the partial differential equations solved simultaneously with the flow. Second, a procedure must be applied to account for the unresolved fluctuations of the velocity, species concentrations, and the temperature, formally to represent the LES spatial averaging (filtering) that is applied to simulate only the largest scales. Even though in theory, the chemistry, the transport properties, and the flame spatial filtering operation are strongly coupled in the LES, so far in practice their modeling has been addressed mostly in a sequential manner. Along these lines, an attempt is made in the present work to consider, at once and in a fully coupled manner, those three basic ingredients (i.e., chemistry downsizing, molecular transport properties, and flame filtering).

Chemistry reduction has been addressed previously, providing reduced chemical schemes (Boivin et al., 2011; Franzelli et al., 2010; Jones and Lindstedt, 1988; Peters, 1985; Westbrook and Dryer, 1984), or from rate-controlled constrained equilibrium (RCCE) (Jones et al., 2003), or with computational singular perturbation (CSP) (Lam and Goussis, 1994), or using chemical look-up tables obtained either from low-dimensional manifold projection (Bykov and Maas, 2007) or from one or multi-dimensional canonical combustion problems, such as flamelets (Hasse and Peters, 2005; Nguyen et al., 2010; van Oijen et al., 2001). All these techniques have benefited from automated optimization tools. In the case of reduced chemistry, it was shown that the rates of global schemes could be found from optimization procedures (Abou-Taouk et al., 2012; Farcy et al., 2014; Polifke et al., 1998; Sikalo et al., 2013; Tham et al., 2008). In the context of look-up table construction, it was also proposed recently to determine with optimization the best fitted progress variable, based potentially on all species of a detailed chemical scheme (Niu et al., 2013; Prufert et al., 2015).

In the continuity of these recent developments, the new approach to sub-grid scale modeling attempted in this article relies on the idea that effects and properties of the spatial filtering, inherent to LES solvers, could be directly accounted for when reducing chemistry and molecular transport properties. A set of reference laminar and one-dimensional premixed flames at various equivalence ratios are first simulated using detailed chemistry. These flames are filtered at a given length scale, which is representative of the one selected in LES of gas turbine subsequently performed. Then, an optimization loop is set up to determine the best molecular diffusion coefficients and Arrhenius rates of a four-step methane-air global mechanism, so that the filtered flame profiles are readily reproduced when the flames are computed over a coarse mesh. This modeling thus

provides a direct estimation of the filtered flame properties from the solution of transport equations at the resolved scale (i.e., over a coarse mesh). Overall, this novel approach is to some extent similar to the thickened flame model (TFLES or TFM) (Boileau et al., 2008; Butler and O'Rourke, 1977; Colin et al., 2000; Kuenne et al., 2012; O'Rourke and Bracco, 1979; Wang et al., 2011). However, in TFLES the flame is simulated by calibrating all species reaction rates and molecular transport properties with the same thickening coefficient, which may vary with turbulence for molecular transport. In the present approach, specific chemical rates and transport properties are automatically derived from optimization tools, so that the nonlinear response of multi-step chemistry to flame spatial filtering is captured accurately by construction. This LES closure is evaluated by simulating a gas turbine reference multi-point injection and partially premixed burner (SGT-100 DLE (Stopper et al., 2010)) and the numerical results are compared against experiments.

The article is organized as follows: the strategy relying on filtered flame response from optimization-based modeling is first presented, then a method for optimizing in spatially filtered flames, molecular transport, and the rates of a four-step global chemistry is discussed, subsequently LES of the multi-point fuel injection burner (using ANSYS CFX) is reported and results are analyzed.

Filtered flame response from optimization-based modeling

Balance equations

The balance equations for the mass fractions Y_i of the N species of a detailed chemical scheme and for temperature, T, may be written in the case of a low Mach number flame (Poinsot and Veynante, 2005):

$$\frac{\partial \rho Y_i}{\partial t} + \nabla \cdot (\rho \mathbf{u} Y_i) = \dot{\Omega}_i = -\nabla \cdot (\rho(\mathbf{V}_i + \mathbf{V}_a) Y_i) + \dot{\omega}_i \tag{1}$$

$$\begin{aligned} \frac{\partial \rho T}{\partial t} + \nabla \cdot (\rho \mathbf{u} T) = \dot{\Omega}_T = \frac{1}{C_p} \nabla \cdot (\lambda \nabla T) - \frac{1}{C_p} \sum_{i=1}^{N} \rho C_{pi} Y_i (\mathbf{V}_i + \mathbf{V}_a) \cdot \nabla T \\ - \frac{1}{C_p} \sum_{i=1}^{N} h_i \dot{\omega}_i \end{aligned} \tag{2}$$

where $\mathbf{u}$ is the velocity vector, ρ is the density. C_{pi} and h_i are the calorific capacity at constant pressure and the enthalpy of the ith species, respectively; λ is the thermal conductivity; and C_p is the calorific capacity of the mixture. The diffusion velocity vector reads: $\mathbf{V}_i = -D_i \nabla X_i / X_i$. D_i is the diffusion coefficient obtained from the Curtiss and Hischfelder (1949) approximation, X_i is the molar fraction of the ith species, $X_i/W = Y_i/W_i$ with W_i and $W = 1/\sum_{k=1,N}(Y_k/W_k)$ the molar weights of the ith species and of the mixture, respectively. (W_i is a constant and W varies with space.) The diffusive flux of mass thus reads: $\rho \mathbf{V}_i Y_i = -\rho D_i (W_i/W) \nabla X_i = -\rho D_i (\nabla Y_i + Y_i (\nabla W/W))$; $\mathbf{V}_a$ is an additional correction velocity ensuring global mass conservation: $\mathbf{V}_a = -\sum_{k=1}^{N} \mathbf{V}_k Y_k = \sum_{k=1}^{N} D_k (\nabla Y_k + Y_k (\nabla W/W))$.

In the relations (1) and (2), $\dot{\Omega}_i$ and $\dot{\Omega}_T$ denote the global contribution of molecular diffusion and reaction to the budgets of the mass fraction and of the temperature. For the

particular case of a propagating planar and unstrained premixed flame, expressing this budget in terms of relative displacement velocity leads to (Peters, 2000):

$$\dot{\Omega}_i = \rho_o(\phi) S_L(\phi) |\nabla Y_i| \text{ and } \dot{\Omega}_T = \rho_o(\phi) S_L(\phi) |\nabla T| \tag{3}$$

where $\rho_o(\phi)$ is the density in the fresh gases and $S_L(\phi)$ the flame speed, both for the equivalence ratio of the mixture ϕ.

A mass weighted Gaussian filtering operation of characteristic filter size Δ is introduced:

$$\bar{\rho}\tilde{Y}_i(\underline{x}, t) = \int_{-\infty}^{+\infty} \rho(\underline{x}', t) Y_i(\underline{x}', t) G_\Delta(\underline{x} - \underline{x}') d\underline{x}' \tag{4}$$

For a given reactive flow, applying this filtering operation to $\rho(\underline{x}, t)$, $Y_i(\underline{x}, t)$, and $T(\underline{x}, t)$, which are the solutions of Eqs. (1) and (2), provides reference detailed chemistry filtered flame solutions $\bar{\rho}^{\text{Ref}}(\underline{x}, t)$, $\tilde{Y}_i^{\text{Ref}}(\underline{x}, t)$, and $\tilde{T}^{\text{Ref}}(\underline{x}, t)$.

In LES, a set of equations is solved in order to approximate these space-filtered aero-thermochemical variables. In the present work, in addition to the momentum equations closed with a sub-grid scale model for turbulent transport, this system of equations is composed of a reduced number $N_s < N$ of equations for chemical species mass fractions, plus an equation for the temperature. These equations include parameters that will be optimized in order to ensure that the solution of a one-dimensional (1D) canonical flame problem, computed over a coarse grid as done in LES, stays very close to the space filtered reference solution $\bar{\rho}^{\text{Ref}}(\underline{x}, t)$, $\tilde{Y}_i^{\text{Ref}}(\underline{x}, t)$, and, $\tilde{T}^{\text{Ref}}(\underline{x}, t)$ of the same problem simulated with detailed chemistry.

Within this context, for a number of $N_s < N$ species reacting according to a reduced global scheme, it is proposed to obtain the filtered distribution of species and temperature by solving:

$$\begin{aligned} \frac{\partial \bar{\rho}\tilde{Y}_i}{\partial t} + \nabla \cdot (\bar{\rho}\tilde{\mathbf{u}}\tilde{Y}_i) = \bar{\dot{\Omega}}_i = -\nabla \cdot \left([\mathbf{V}_i^{\text{Op}}(\tilde{\phi}, \underline{\tilde{Y}}) + \mathbf{V}_a^{\text{Op}}(\tilde{\phi}, \underline{\tilde{Y}})] \tilde{Y}_i \right) \\ + \Xi \dot{\omega}_i^{\text{Op}}(\tilde{\phi}, \underline{\tilde{Y}}, \tilde{T}) \end{aligned} \tag{5}$$

$$\begin{aligned} \frac{\partial \bar{\rho}\tilde{T}}{\partial t} + \nabla \cdot (\bar{\rho}\tilde{\mathbf{u}}\tilde{T}) = \bar{\dot{\Omega}}_T = \frac{1}{C_p} \nabla \cdot (\lambda^{\text{Op}}(\tilde{\phi}) \nabla \tilde{T}) \\ - \frac{1}{C_p} \sum_{i=1}^{N} \rho C_{pi} Y_i \left[\mathbf{V}_i^{\text{Op}}(\tilde{\phi}, \underline{\tilde{Y}}) + \mathbf{V}_a^{\text{Op}}(\tilde{\phi}, \underline{\tilde{Y}}) \right] \cdot \nabla \tilde{T} \\ - \frac{1}{C_p} \Xi \sum_{i=1}^{N} h_i \dot{\omega}_i^{\text{Op}}(\tilde{\phi}, \underline{\tilde{Y}}, \tilde{T}) \end{aligned} \tag{6}$$

The filtered diffusion velocities and chemical rates are expressed with $\mathbf{V}_i^{\text{Op}}(\tilde{\phi}, \underline{\tilde{Y}})$, $\lambda^{\text{Op}}(\tilde{\phi})$, and $\dot{\omega}_i^{\text{Op}}(\tilde{\phi}, \underline{\tilde{Y}}, \tilde{T})$, which are optimized functions of the equivalence ratio, of the vector of species mass fractions, and of the temperature. Accordingly, it is proposed to write the diffusion velocity, the thermal conductivity, and the burning rate of Eqs. (5) and (6) in the form:

$$\mathbf{V}_i^{\mathrm{Op}}\left(\tilde{\phi},\underline{\tilde{Y}}\right) = -F^{\mathrm{OpD}}\left(\tilde{\phi}\right)D_i\left(\underline{\tilde{Y}}\right)\frac{\nabla\tilde{X}}{\tilde{X}_i} \tag{7}$$

$$\lambda^{\mathrm{Op}}\left(\tilde{\phi}\right) = F^{\mathrm{OpD}}\left(\tilde{\phi}\right)\lambda\left(\underline{\tilde{Y}},\tilde{T}\right) \tag{8}$$

$$\begin{aligned}\dot{\omega}_i^{\mathrm{Op}}\left(\tilde{\phi},\underline{\tilde{Y}},\tilde{T}\right) = {} & F^{\mathrm{OpR}}\left(\tilde{\phi}\right)W_i\sum_{j=1}^{N_r}\left(\mu_{i,j}^{b}-\mu_{i,j}^{f}\right)\\ & \times A_j\prod_{k\in\mathcal{A}_j}\left(\frac{\bar{\rho}\tilde{Y}_k}{W_k}\right)^{\nu_{k,j}}\tilde{T}^{B_j}\exp\left(-E_{a_j}\Big/\left(\mathcal{R}\tilde{T}\right)\right)\end{aligned} \tag{9}$$

where $\mathcal{A}_j$ is the ensemble of species involved in the jth chemical reaction; $\mu_{i,j}^{f}$ (resp. $\mu_{i,j}^{b}$) are the forward (resp. backward) stoichiometric coefficients of the jth reaction rate; and N_r is the number of global chemical steps considered. The two functions of the equivalence ratio $F^{\mathrm{OpD}}\left(\tilde{\phi}\right)$ and $F^{\mathrm{OpR}}\left(\tilde{\phi}\right)$ along with the pre-exponential factor, A_j, the temperature exponent, B_j, the activation energy, E_{aj}, and $\nu_{i,j}$, the reaction orders of species i in reaction j must be determined.

These functions and parameters need to be optimized so that the flame solution obtained with Eqs. (5) and (6) matches the solution $\bar{\rho}^{\mathrm{Ref}}(\underline{x},t)$, $\tilde{Y}_i^{\mathrm{Ref}}(\underline{x},t)$, and $\tilde{T}^{\mathrm{Ref}}(\underline{x},t)$, which are the Gaussian filtered distribution of the solution of the primitive equations (1) and (2). In the case of a planar flame, the parameter Ξ is set to unity; however, in the turbulent flame, Ξ takes the form of a sub-grid scale wrinkling factor (Wang et al., 2011). Nevertheless, in the present work the flame resolution by the mesh must be high enough so that the sub-grid scale fluctuations are more controlled by the thickening of the flame due to flame filtering than by sub-grid scale wrinkling of the flame surface, therefore, Ξ will stay very close to unity.

The filtered molecular diffusion and reaction rate budgets obviously depart from their unfiltered expressions. Specifically, the nonlinear burning rates, once filtered and examined in composition space (i.e., versus filtered species mass fractions and filtered temperature), cannot exactly feature an Arrhenius-type response. However, turbulent combustion models explicitly using Arrhenius expressions, as the thickened flame model (Boileau et al., 2008; Colin et al., 2000; Gicquel et al., 2012; Kuenne et al., 2012) have been successful in many applications. This may be explained by the fact that these modeling approaches provide fair estimations of the global budgets $\dot{\bar{\Omega}}_i$ (Eq. (5)) and $\dot{\bar{\Omega}}_T$ (Eq. (6)), which reproduce the proper flame speed and ensures species profiles resolution. It is worthwhile to note that, in practice, ensuring flame speed and species profiles resolution may be more useful than an accurate treatment of an isolated filtered source term, which is then introduced into a balance equation that is not calibrated to reproduce, over the coarse mesh, any of the expected asymptotic filtered flame behaviors.

Optimization procedure

First, a set of N_{fl} 1D and unstrained premixed flames are computed with a detailed chemical scheme. This is done for an ensemble of operating conditions, characterized for instance by the equivalence ratio and the fresh gases temperature. This solution is spatially filtered at a given length scale Δ, to provide a reference solution. Second, the same set of flames is

simulated solving for Eqs. (5) and (6). A fitness function to be minimized and measuring the departure between the two set of solutions may be written:

$$\mathcal{F}_Y\left(\left(A_j, B_j, E_{aj}, \mu_{i,j}\right)_{j=1,N_r;\ i=1,N_S}, F^{\mathrm{OpD}}\left(\tilde{\phi}\right), F^{\mathrm{OpR}}\left(\tilde{\phi}\right)\right) = \sum_{\ell=1}^{N_{\mathrm{fl}}}\left[\sum_{i=1}^{N_S}\sum_{k=1}^{N_p}\frac{\left|\tilde{Y}_{\mathrm{i}}\left(x^k;\ell\right)-\tilde{Y}_i^{\mathrm{Ref}}\left(x^k;\ell\right)\right|}{\tilde{Y}_i^{\mathrm{Ref}}\left(x^k;\ell\right)}+\beta\left(\frac{\left|S_L^{\mathrm{Ref}}(\ell)-S_L(\ell)\right|}{S_L^{\mathrm{Ref}}(\ell)}\right)\right] \tag{10}$$

N_p is the number of solution points per flame. As introduced above, N_{fl} is the number of reference flames and N_{s} the number of chemical species involved in the N_r reaction steps. β is the relative weight given to the flame speed prediction. After defining ranges of search for all the parameters, well-established multi-objective optimization approaches, as those relying on the simplex or interior point methods (Vanderbei, 2001) or again genetic algorithm (Razali and Geraghty, 2011), may be applied to find the best set of parameters for the considered conditions. Flames are then solved interactively with the optimization tools, until $\mathcal{F}_Y$ reaches its minimum determining the best set of parameters.

The fitness function (10) combines the optimization of molecular diffusion and Arrhenius rates. This choice was made because it was not possible to match, for a range of equivalence ratios, both the slope of the filtered profiles and the flame speed by acting only on the diffusive fluxes (i.e., keeping unaltered the reaction rates).

Application to premixed methane-air filtered flames

In a first test of this new approach applied to methane-air combustion, the chosen global mechanism to be optimized is composed of four reactions, which are given in Table 1: (i) the fuel oxidation into CO and H_2; (ii) H_2 and O_2 into H_2O; (iii) CO and O_2 into CO_2; and (iv) the water gas shift reaction, i.e., CO and H_2O into CO_2 and H_2. Such global schemes have been discussed at many occasions in the literature and for various hydrocarbon fuels. Only major flame properties may be reproduced by these global chemical schemes (Abou-Taouk et al., 2012, 2013; Jones and Lindstedt, 1988; Marzouk and Huckaby, 2010; Meredith and Black, 2006; Novosselov and Malte, 2008; Slavinskaya and Unkhoff, 2008; Westbrook and Dryer, 1984); however, for unsteady flow simulations in complex geometries, they offer an interesting alternative to single-step chemistry, or to tabulated chemistry, which may be difficult to handle in the case of multiple injections leading to large lookup tables requiring a huge amount of computing memory. The seven species involved allow for reproducing the adiabatic flame temperature over the range of equivalence ratios considered, as illustrated in Figure 1.

Table 1. Optimized global chemical scheme (units in cm, s, kcal, and mol) for the 1 bar and 3 bar cases.

Reaction	A_j	B_j	E_{a_j}	Reaction order
$CH_4+\frac{1}{2}O_2 \rightarrow CO+2H_2$	9.213E+14	0	31.5	$[CH_4]^{0.62}, [O_2]^{1.5}$
$H_2+\frac{1}{2}O_2 \rightarrow H_2O$	1.606E+18	−1.2	40.67	$[H_2]^{0.425}, [O_2]^{1.694}$
$CO+\frac{1}{2}O_2 \rightarrow CO_2$	1.746E+15	0	40.6	$[CO]^{1.05}, [O_2]^{0.3}, [H_2O]^{0.5}$
$CO+H_2O \leftrightarrow CO_2+H_2$	1.305E+15	0	20.5	$[CO], [H_2O]$

N_2 is also present in the mixture as an inert species.

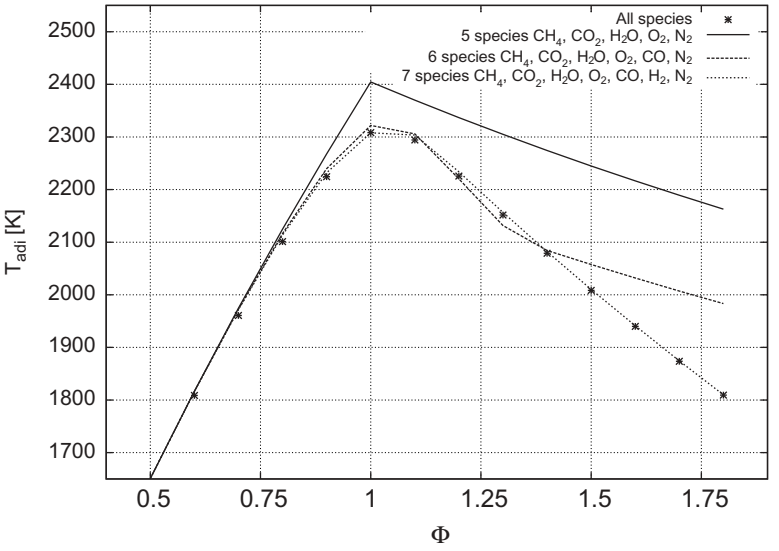

Figure 1. Adiabatic flame temperature vs. equivalence ratio for different sets of chemical species, $T_o = 650\,\mathrm{K}$, $P_o = 1\,\mathrm{bar}$. Symbols: 53 species. Line: 5 species $CH_4, CO_2, H_2O, O_2, N_2$. Dash line: 5 species + CO. Dotted-line: 5 species + CO and H_2.

A set of $N_{\mathrm{fl}} = 18$ freely propagating methane-air premixed flames are simulated with the GRI-Mech 3.0 (Smith et al., 1999) detailed chemistry and the mixture averaged transport coefficients (Curtiss and Hischfelder, 1949). The 18 flames are decomposed for the two fresh gas temperatures, $T_o = 300$ K and 650 K, into 9 flames equally distributed in equivalence ratio within the range $\phi \in [0.4,\ 1.2]$. These laminar flamelets are Gaussian filtered at $\Delta = 1$ mm, and the resulting database stored as a reference. This filter size corresponds to $2 < \Delta/\delta_L(\phi) < 5$, with $\delta_L(\phi)$ an estimation of the flame thickness at the given equivalence ratio ϕ. Indeed, with $T_o = 650$K and under a pressure of 3 bar (conditions of the gas turbine simulations reported thereafter), the thickness of flames based on the temperature gradient varies between $\delta_L = 0.50$mm on the lean side down to 0.25 mm under the stoichiometric condition. The ratio Δ/δ_L is intentionally kept small so that eventual sub-grid scale flame wrinkling also stays limited, the need for sub-grid scale modeling is therefore mainly driven by the flame thickening effect over the LES mesh. The software CHEMKIN (2015) has been modified to solve Eqs. (5) and (6), and it was coupled with the optimization toolbox mode-FRONTIER (2015), to end up with the best fit for the parameters according to the fitness function $\mathcal{F}_Y$, as given by Eq. (10). The value $\beta = 3$ has been retained to calibrate the importance of flame speed accuracy.

To initialize the optimization loop, random points are selected within ranges of parameters defined in Table 2. The range for the chemical rates has been determined from previous four-step methane/air chemistry (Abou-Taouk et al., 2013), the range of the correction to molecular diffusion was chosen so that it would correspond to a flame thickening factor varying between unity and 10. For the present optimization process, 7000 sets of parameters are systematically evaluated within these ranges. Flame simulations, solving Eqs. (5) and (6) with $\Xi = 1$, are organized interactively with the optimization toolbox to dynamically test parameters values till convergence. This optimization

Table 2. Maximum and minimum bounds for parameters during optimization.

Parameter	Minimum	Maximum
A_1, A_3, A_4	$1{\cdot}10^{12}$	$5{\cdot}10^{15}$
A_2	$1{\cdot}10^{16}$	$5{\cdot}10^{18}$
F^{OpR}	0.10	2.00
B_1, B_3, B_4	−0.50	0.50
B_2	−1.50	−0.50
E_{a1}, E_{a2}, E_{a3}	20.00	50.00
E_{a4}	15.00	40.00
$\mu_{j,i}$	0.25	1.70
F^{OpD}	1.00	10.00

process minimizes the fitness function defined in relation (10), which is used to discriminate between the solutions by measuring the error on the filtered species, flame speed, and temperature. In addition, the solutions are assumed fully converged when errors on flame speed are below 5%.

The rates of the reduced chemical schemes obtained with this method are given in Table 1; it takes about 2 days to reach convergence on a desktop computer. The two functions $F^{\mathrm{OpD}}(\phi)$ and $F^{\mathrm{OpR}}(\phi)$ are plotted in Figure 2. In view of the gas turbine application reported below, both cases under atmospheric pressure and with the pressure set at $P_o = 3$ bar have been considered. For these two pressure conditions, the responses versus equivalence ratio of the functions $F^{\mathrm{OpD}}(\phi)$ and $F^{\mathrm{OpR}}(\phi)$ differ. At 3 bar, F^{OpD} increases with equivalence ratio, from $F^{\mathrm{OpD}}(\phi = 0.4) = 3.2$ up to $F^{\mathrm{OpD}}(\phi = 1.2) = 6.5$ (Figure 2), while it decreases from 6.6 down to about 1.7 at one bar for the same range of equivalence ratios. F^{OpR} increases with equivalence ratio at a pressure of one bar (from 0.9 up to 2.1) and decreases at 3 bar (from 0.5 down to 0.2). However, it was found possible to incorporate all of the pressure effects within these parameters and to keep the remaining

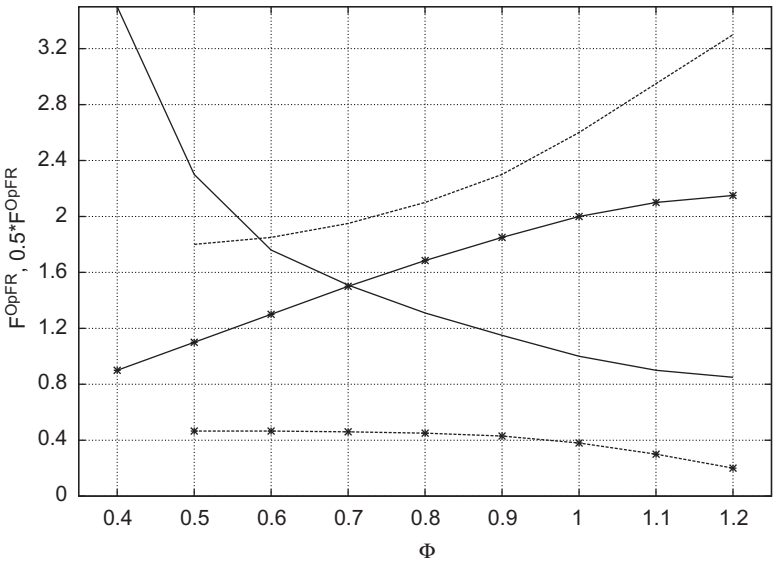

Figure 2. Diffusion functions vs. equivalence ratio. Line: $0.5 \times F^{\mathrm{OpD}}$. Line with symbols: F^{OpR}. Solid line: $P_o = 1$ bar. Dashed line: $P_o = 3$ bar.

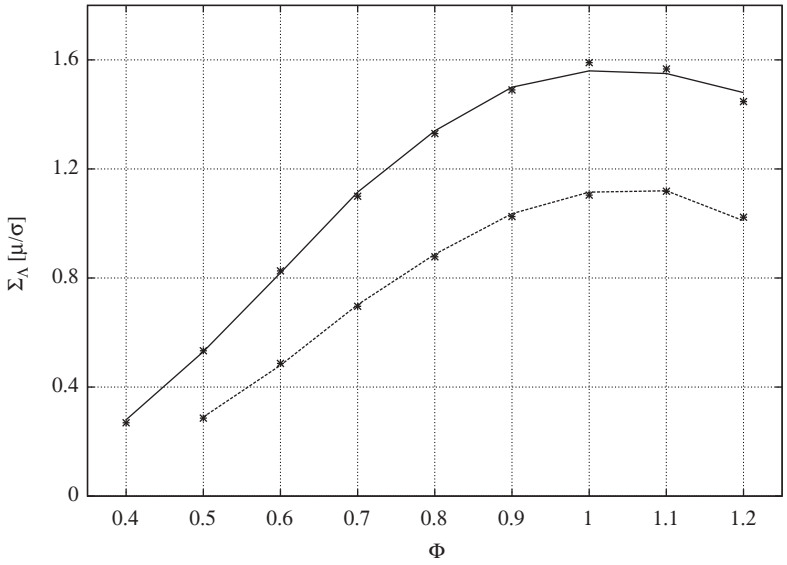

Figure 3. Flame speed vs. equivalence ratio. Symbols: $S_L^{\mathrm{Ref}}(\phi)$ (GRI-mech). Line: $S_L(\phi)$ solving Eqs. (5) and (6) with optimized filtered chemistry. $T_o = 650$ K. Solid line: $P_o = 1$ bar. Dashed line: $P_o = 3$ bar.

chemical parameters the same (Table 1) for the two pressure levels studied. Even though the parameters can be optimized for a given mean pressure, few applications are isobaric. Nevertheless, the sensitivity of the results with pressure are, in the present case, in line with those expected in simulations with such simplified four-step description of chemistry.

Figure 3 shows the flame speed for both cases at atmospheric pressure and 3 bar. The optimization loop has provided a system of equations, which propagate the flame front at the flame speed obtained with the detailed chemical scheme. At this point it is important to note that using another, eventually improved, detailed chemical scheme would change the reference values, but without any impact on the method proposed to reproduce them with the automated optimization procedure. Figures 4 and 5 show reference profiles of Gaussian filtered temperature and species concentrations at different equivalence ratios, together with the profiles obtained using the modeled equations. Concerning temperature profiles seen in Figure 4, the slopes of the filtered profiles are well reproduced by the modeled equations, and it is confirmed that the reduced scheme leads to a very reasonable estimation of the burned gases temperature; at $\phi = 0.5$ an under prediction of about 13 K is observed, at $\phi = 1$ an over prediction of 1 K, at $\phi = 1.1$ an over prediction of 10 K, and at $\phi = 1.2$ an over prediction of 14 K (the last two conditions are not shown in the plots for brevity). An overshoot of the temperature in the transition toward fully burned gases is unavoidable with only seven species and it is indeed seen in all of the temperature responses obtained with the optimized four-step global scheme. It is also observed that the modeling properly captures most of the equilibrium conditions for species (see Figure 5), except on the rich side. Here also, more intermediate radical species would be needed to better match the detailed chemistry. Nevertheless, the slopes of the filtered profiles are reproduced quite well (i.e., the expected filtered thickness of the species

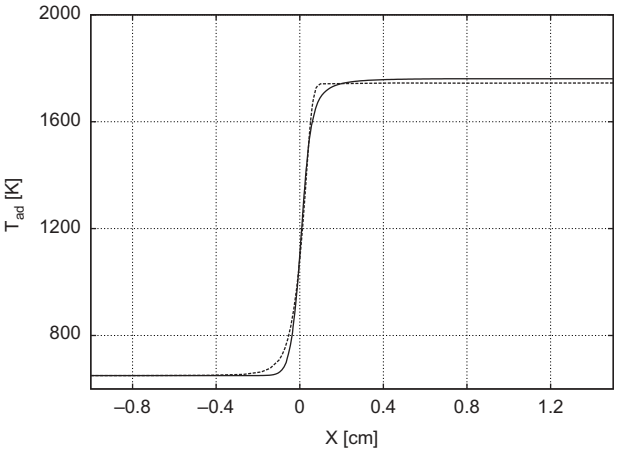

(a) $\phi = 0.5$

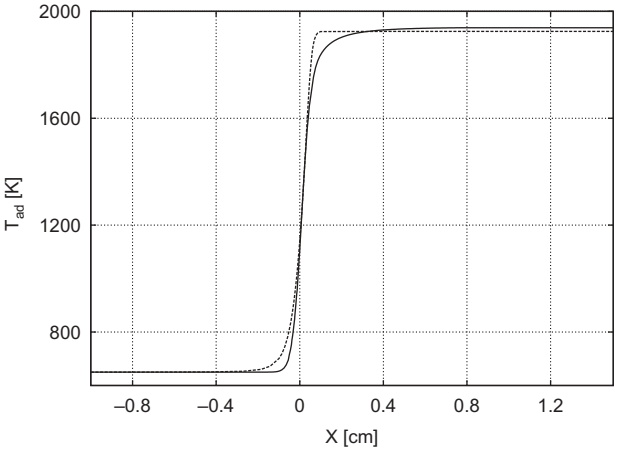

(b) $\phi = 0.6$

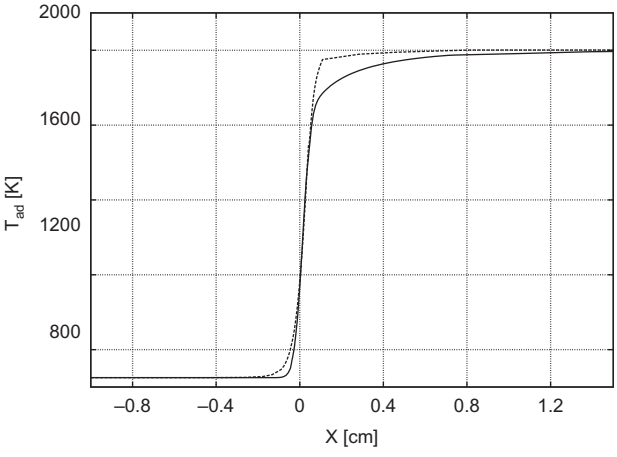

(c) $\phi = 1.0$

Figure 4. Filtered temperature profiles vs. position for different ϕ. Line: $\tilde{T}^{\mathrm{Ref}}(x)$ reference filtered flame (GRI-Mech). Dashed line: $\tilde{T}(x)$ from modeled Eqs. (6), (5). $P_o = 1\,\mathrm{bar}$, $T_o = 650\,\mathrm{K}$, and $\Delta = 1\,\mathrm{mm}$.

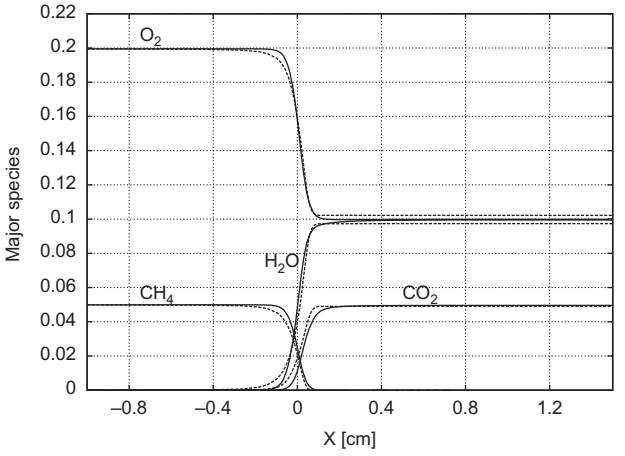

(a) $\phi = 0.5$

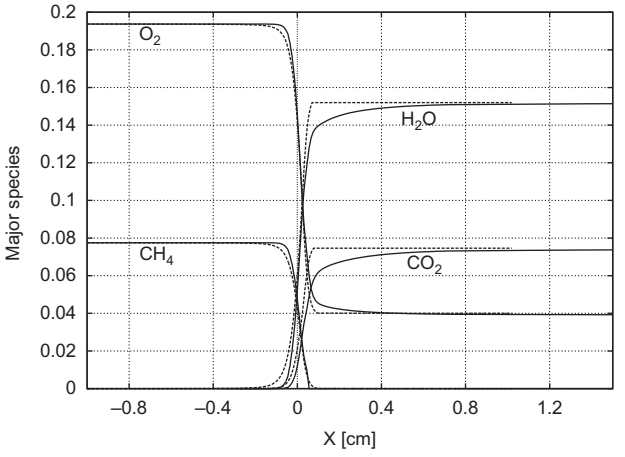

(b) $\phi = 0.8$

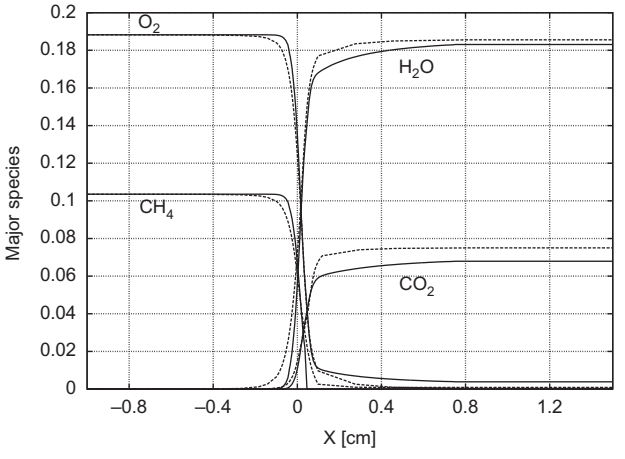

(c) $\phi = 1.1$

Figure 5. Filtered species profiles vs. position. Line: $\tilde{Y}_i^{\mathrm{Ref}}(x)$ reference filtered flame (GRI-Mech). Dashed line: $\tilde{Y}_i$ from modeled Eqs. (6), (5). $P_o = 1\,\mathrm{bar}$, $T_o = 650\,\mathrm{K}$, and $\Delta = 1\,\mathrm{mm}$.

distributions), specifically considering the complexity of the nonlinear coupling between detailed chemistry and space filtering that needs to be captured.

Only a four-step mechanism has been targeted in this first attempt of optimization and, therefore, some departure to the detailed chemistry was expected, but it is confirmed that the overall filtered flame structure is readily obtained solving Eqs. (5) and (6). At this stage, a set of closed equations is available to simulate the dynamics of filtered flames, ensuring that major flame responses are similar to the ones observed after filtering a flame computed with a reference fully detailed chemistry. This modeling approach is now applied to a partially premixed burner, in which most of the reaction zones operate in a premixed mode, i.e., with fluxes across equivalence ratio surfaces at the flame front expected much smaller than the fluxes in the direction normal to the reaction zone, therefore allowing for using the calibration of chemistry from the collection of premixed flames.

LES of a multi-point swirling injector

The SGT-100 is an industrial gas turbine designed and manufactured at Siemens Industrial Turbomachinery Ltd, UK, which features dual-fuel capability. The combustor was experimentally investigated at DLR (Deutsches Zentrum fûr Luft- und Raumfahrt) (Stopper et al., 2010). The system consists of a main burner, pilot burner, radial swirler, and double-skinned can combustor; a sketch is given in Figure 6 (Stopper et al., 2010). Gaseous fuel is injected from two different locations. There are 12 main injection holes at the entrance of the swirler slot and two gas injection holes on the side wall of each swirler vane. This burner geometry has been studied previously with RANS (Reynolds Averaged Navier Stokes) (Abou-Taouk et al., 2013), hybrid RANS/LES (Abou-Taouk et al., 2013, 2015), scalar dissipation rate model (Sadasivuni et al., 2012), and with LES (Bulat et al., 2013, 2014, 2015a, 2015b).

In the DLR test rig (Stopper et al., 2010, 2013), the burner is fitted to a square combustion chamber with quartz windows (see Figure 6 for the experimental setup and Figure 7a for an overall view of the flow). The air is supplied through the circumferential inlet around the swirler, inside of which the fuel (German natural gas consisting of 96.97% of CH_4) is injected at various injectors in the swirl generator (36 holes). The flow is turned through the swirler vanes into the prechamber, where the air and fuel mixture exits into

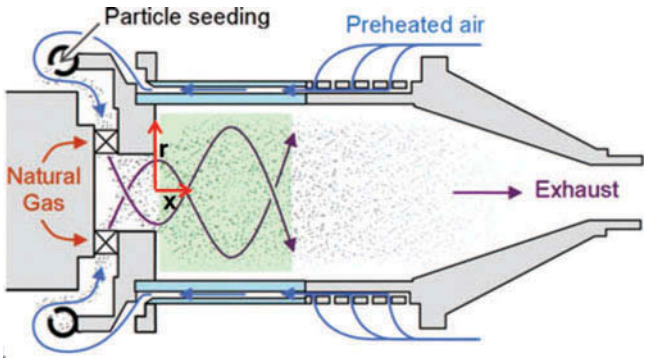

Figure 6. Sketch of the experimental setup (Stopper et al., 2010).

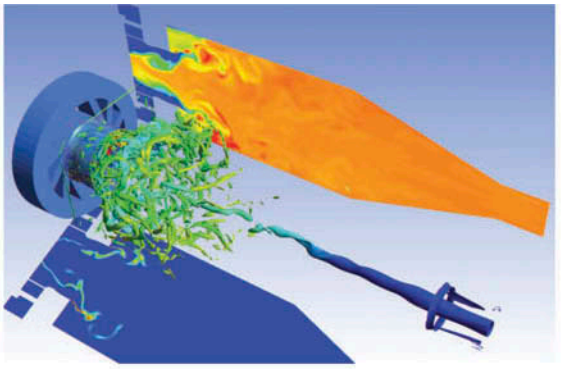

(a) 3D view of the swirling flame

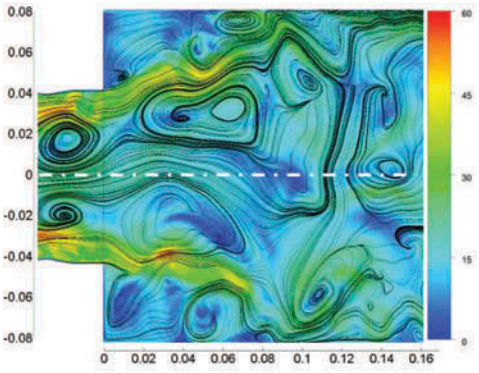

(b) Streamline centerline plane

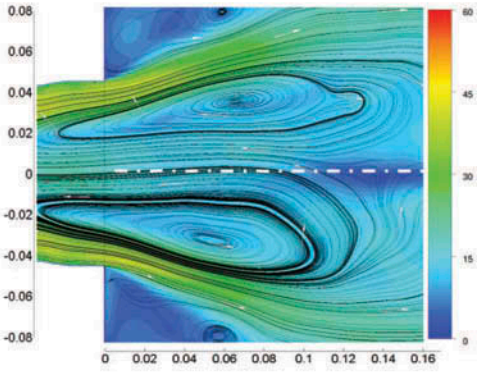

(c) Averaged streamline centerline plane

Figure 7. (a) iso-Q ($Q = 1{\cdot}10^7$). Bottom plane: heat release rate. Back plane: temperature normalized by its maximum. (b) Streamline colored by velocity magnitude (m/s). (c) Averaged streamline colored by velocity magnitude (m/s).

the square combustion chamber. One-dimensional Raman for scalar and particle image velocimetry (PIV) velocity measurements profiles are available at four streamwise locations (Stopper et al., 2010).

Specified mass flow rates are imposed at the inlet boundaries for the main air inlet, burner panel inlet, and the 36 fuel inlets. The preheated air temperature is set to 685 K at the air inlets and 320 K for the fuel inlets. The outlet boundary condition is set to 3 bar and a no-slip adiabatic condition is imposed on all walls. The total equivalence ratio in the burner is approximately 0.59. The cooling air inlet that was used in experiments to cool the surface walls of the square combustor can and conical duct is neglected in the simulations.

The Navier Stokes equations are solved with the energy and above species mass fraction balance equations. The transport of momentum by unresolved velocity fluctuations is expressed with the WALE model (Nicoud and Ducros, 1999). The ANSYS CFX software is used based on the finite volume method with a pressure-velocity coupled solver and a time-implicit bounded second-order upwind biased discretization of the equations. The mesh is composed of 24.5 million hexahedral cells, leading to a characteristic resolution length h within the flame zone 0.30 mm $< h <$ 0.40 mm, to be compared with the laminar flame thickness discussed above: 0.25mm $< \delta_L <$ 0.5 mm ($T_o = 650$ K and $P_o = 3$ bar).

Therefore, the flame cannot be fully resolved by the mesh and some filtering is indeed needed. However, and as discussed previously, because the filter size applied to the laminar flame for calibration is such that $2 < \Delta/\delta_L < 5$, sub-grid flame wrinkling cannot be much pronounced and only a weak level of 5% of unresolved wrinkling is arbitrarily allowed ($\Xi = 1.05$) in Eqs. (5) and (6).

The statistics are first converged for a nonreactive case, the flow is then advanced in time with combustion for about seven flow-through times until the flame is well established and statistics are accumulated for another seven flow-through times. The time step for the simulation was set to 1 μs, which implies an averaged Courant–Friedrich–Levy (CFL) number of 0.5. The simulation was performed using 112 processors.

Figure 7a shows a 3D view of the flow. Some of the simulated vortex filaments are visualized with the Q-criterion along with transverse planes of temperature and burning rate. In the prechamber, the fuel is distributed close to the cylindrical wall after being injected in the radial swirlers. It is seen in Figure 7b that a vortex is created close to the wall between the burner exit and the chamber wall, due to a sudden expansion from the prechamber. In this region, the fuel is found in high concentration. The axial RMS velocity fluctuations are high within the high-speed flow regions in the prechamber, which then discharges into the combustion chamber.

The flow field also shows a central vortex core (CVC) of high axial velocity, protruding backwards from the outlet plane into the transition duct. This strong CVC has been reported in the experiments (Stopper et al., 2013), where this phenomenon is explained by a Rankine-type vortex. The central recirculation zone is found inside the flame shear layers, and an outer recirculation zone can be observed between the high-speed flow entering the combustion chamber wall. From the instantaneous velocity field, it is seen that the inner shear layer consists of small vortices that are created and then disappear. The vortex field visible in the instantaneous flow field is not steady, but rather is observed to move backward and forward. The radial extents as well as the opening angle in the region of $x < 0.08$ m are similar to the experimental measurements. The outer shear layer, where the highest velocity gradients are obtained, can be defined as the outer layer ($|r| > 0.042$ m) in the vicinity of the burner ($x < 0.065$ m).

The flame is stabilized in the prechamber, while the greatest combustion activity occurs in the form of a hollow cone that extends outwards into the combustion chamber. As is typical of all industrial combustors, the mode of combustion is not perfectly premixed but may be characterized as an ensemble of flamelets with a range of different equivalence ratios. The total pressure drop across the combustor is approximately 0.9% of the combustor mean pressure of 3 bar, which is in acceptable agreement with the experimentally measured pressure drop of the order of 1% across the combustor (Stopper et al., 2010).

Statistical results are compared in Figure 8 against the measurements and previous numerical results obtained with an hybrid URANS/LES approach, in which turbulent combustion is modeled with an eddy dissipation closure (Magnussen, 1981) combined with a global reduced chemistry (Abou-Taouk et al., 2012). In terms of the statistical properties of the velocity field, the present simulations provide results that are overall closer to measurements at the first two sections, a better agreement which is more pronounced for the spanwise averaged velocity even further downstream (Figure 8b). The average temperature (Figure 8c) and CO_2 mass fraction (Figure 8d) are quite well

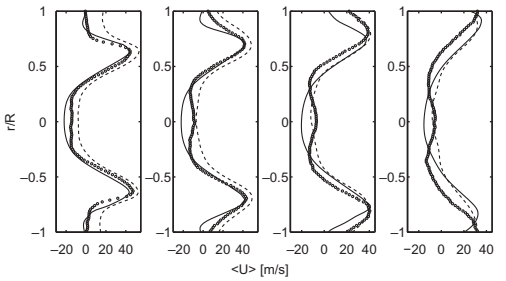

(a) Streamwise averaged velocity

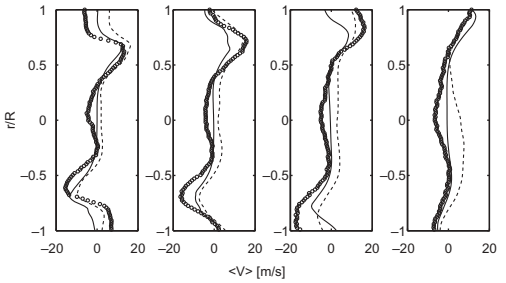

(b) Spanwise averaged velocity

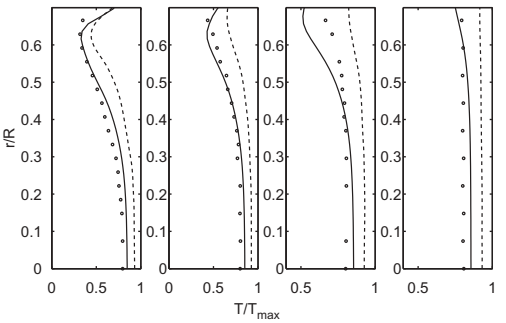

(c) Averaged temperature

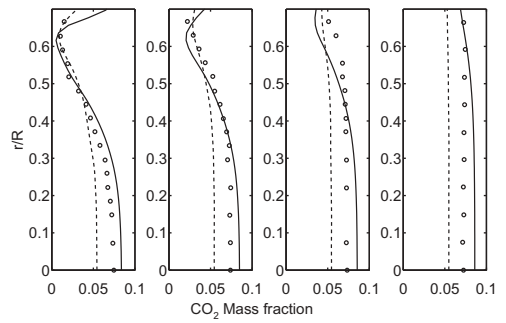

(d) Averaged CO_2 mass fraction

Figure 8. Symbol: Experiments (Stopper et al., 2010). Solid-line: present LES. Dashed-line: hybrid URANS/LES from Abou-Taouk et al. (2012). The four locations correspond to x = 0.025, 0.045, 0.065, and 0.095 (meter) in Figures 7b and 7c.

reproduced with the new LES modeling approach; both the amplitudes and the shape of the profiles are very close to measurements for all locations, and this was not the case with the previous computations.

Summary

A novel approach for large eddy simulation (LES) of turbulent flames has been discussed. The proposed method relies on the solving of first principle balance equations for species mass fractions and energy, but with chemical rates and molecular transport resulting from an optimization procedure. This optimization is organized so that the solution of canonical flame problems, addressed with a limited number of species, matches a reference spatially filtered solution obtained with a detailed chemical scheme. Therefore, the optimized first principle equations readily provide the expected Gaussian filtered flame solution over the LES mesh. To be valid, this approach must be combined with a good mesh resolution, typically the ratio between the characteristic length of the filter applied to the flame and the flame thickness is below five in the present work.

In the case of methane/air combustion, the parameters of a four-step global chemical scheme, with its corresponding transport properties, have been automatically obtained from the optimization loop for a range of equivalence ratios and two levels of pressure. The optimized rates and molecular diffusion fluxes allow for capturing the flame speed response versus equivalence ratio and the Gaussian filtered profiles of major species, as provided by the GRI detailed chemistry. The flame solution is, therefore, sufficiently thick to be resolved over a coarse LES grid, but preserving by construction the nonlinear interaction between the Gaussian filter and the seven chemical species involved in the reduced mechanism. Then, this LES modeling is applied to an industrial gas turbine and the flow statistical properties are compared against measurements and previous numerical simulations (Abou-Taouk et al., 2012).

In future works, the optimization may be refined by adding the kinetic pressure effects directly in the set of chemistry parameters, through a third-body type of reaction. Also, the optimization of the chemical rates and of the molecular properties to match filtered reference profiles, may be combined with an automated reduction of the chemistry itself, as directed relation graph with error propagation (Lu and Law, 2005).

Acknowledgments

The authors would like to acknowledge Dr. G. Bulat and Dr. D. Lörstad from Siemens for helpful discussions concerning the industrial test case.

Funding

This work was funded by the Swedish Energy Agency, Siemens Industrial Turbomachinery AB, Finspong, Sweden, GKN Aerospace Engine Systems Sweden, and the Royal Institute of Technology through the Swedish research program TURBO POWER. The second author was funded by ANRT (Agence Nationale de la Recherche et de la Technology) and Solvay-Rhodia under CIFRE No. 73683.

References

Abou-Taouk, A., Sadasivuni, S., Lörstad, D., Bulat, G., and Eriksson, L.-E., 2015. CFD analysis and application of dynamic mode decomposition for resonant-mode identification and damping in

an SGT-100 DLE combustion system. In *Proceedings of the European Combustion Meeting*, Paper P4–46, Budapest, Hungary, March 30–April 2

Abou-Taouk, A., Sigfrid, I., Ronald, W., and Eriksson, L.-E. 2012. A four-step global reaction mechanism for CFD simulations of flexi-fuel burner for gas turbines. In *Turbulence, Heat and Mass Transfer 7*, Palermo, Italy, September 24–27, pp. 785–788.

Abou-Taouk, A., Suresh, S., Daniel, L., and E, L.-E. 2013. Evaluation of global mechanisms for LES analysis of SGT-100 DLE combustion system. Presented at ASME Turbo Expo 2013, San Antonio, TX, June 3–7.

Boileau, M., Staffelbach, G., Cuenot, B., Poinsot, T., and Bérat, C., 2008. LES of an ignition sequence in a gas turbine engine. *Combust. Flame*, **154**(1–2), 2–22.

Boivin, P., Jiménez, C., Sánchez, A.L., and Williams, F.A., 2011. An explicit reduced mechanism for H_2 air combustion. *Proc. Combust. Inst.*, **33**(1), 517–523. ISSN 1540-7489.

Boudier, G., Gicquel, L.Y.M., and Poinsot, T.J., 2008. Effects of mesh resolution on large eddy simulation of reacting flows in complex geometry combustors. *Combust. Flame*, **155**(1–2), 196–214.

Bulat, G., Fedina, E., Fureby, C., Meier, W., and Stopper, U. 2015a. Reacting flow in an industrial gas turbine combustor: LES and experimental analysis. *Proc. Combust. Inst.*, **35**(3), 3175–3183.

Bulat, G., Jones, W., and Marquis, A., 2013. Large eddy simulation of an industrial gasturbine combustion chamber using the sub-grid PDF method. *Proc. Combust. Inst.*, **34**(2), 3155–3164.

Bulat, G., Jones, W.P., and Marquis, A.J. 2014. NO and CO formation in an industrial gas-turbine combustion chamber using LES with the Eulerian sub-grid PDF method. *Combust. Flame*, **161**(7), 1804–1825.

Bulat, G., Jones, W. P., and Navarro-Martinez, S. 2015b. Large eddy simulations of isothermal confined swirling flow in an industrial gas-turbine. *Int. J. Heat Fluid Flow*, **51**, 50–64.

Butler, T. D., and O'Rourke, P. J. 1977. A numerical method for two-dimensional unsteady reacting flows. *Symp. (Int.) Combust.*, **16**, 1503–1515.

Bykov, V., and Maas, U. 2007. The extension of the ILDM concept to reaction-diffusion manifolds. *Combust. Theor. Model.*, **11**(6), 839–862.

CHEMKIN. 2015. Available at: http://www.reactiondesign.com.

Colin, O., Ducros, F., Veynante, D., and Poinsot, T. 2000. A thickened flame model for large eddy Simulations of turbulent premixed combustion. *Phys. Fluids*, **12**(7), 1843–1863.

Curtiss, C. F., and Hischfelder, J. O. 1949. Transport properties of multicomponent gas mixtures. *J. Chem. Phys.*, **17**, 550.

Domingo, P. and Vervisch, L. 2015. Large eddy simulation of premixed turbulent combustion using approximate deconvolution and explicit flame filtering. *Proc. Combust. Inst.*, **35**(2), 1349–1357.

Farcy, B., Abou-Taouk, A., Vervisch, L., Domingo, P., and Perret, N. 2014. Two approaches of chemistry downsizing for simulating selective non catalytic reduction DeNOx process. *Fuel*, **118**, 291–299.

Ferziger, J. H. 1993. Subgrid scale modeling. In *Large Eddy Simulation of Complex Engineering and Geophysical Flows*, Cambridge University Press, pp. 37–54.

Fiorina, B., Vicquelin, R., Auzillon, P., Darabiha, N., Gicquel, O., and Veynante, D. 2010. A filtered tabulated chemistry model for LES of premixed combustion. *Combust. Flame*, **157**, 465–475.

Franzelli, B., Riber, E., Sanjose, M., and Poinsot, T. 2010. A two-step chemical scheme for kerosene-air premixed flame. *Combust. Flame*, **157**(7), 1364–1373.

Gicquel, L. Y. M., Staffelbach, G. and Poinsot, T. 2012. Large eddy simulations of gaseous flames in gas turbine combustion chambers. *Prog. Energy Combust. Sci.*, **38**(6), 782–817.

Hasse, C., and Peters, N. 2005. A two mixture fraction flamelet model applied to split injections in a DI diesel engine. *Proc. Combust. Inst.*, **30**, 2755–2762.

Jones, W. P., and Lindstedt, R. P. 1988. Global reaction schemes for hydrocarbon combustion. *Combust. Flame*, **73**, 233–249.

Jones, W. P., Rigopoulos, S., Smith, S., and Maas, U. 2003. Reduction of comprehensive chemistry via constraint potentials. *Proc. Combust. Inst.*, **30**(1), 1325–1331.

Kuenne, G., Seffrin, F., Fuest, F., Stahler, T., Ketelheun, A., Geyer, D., Janicka, J., and Dreizler, A. 2012. Experimental and numerical analysis of a lean premixed stratified burner using 1D Raman/Rayleigh scattering and large eddy simulation. *Combust. Flame*, **159**(8), 2669–2689.

Lam, S. H., and Goussis, D. A. 1994. The CSP method for simplifying kinetics. *Int. J. Chem. Kinet.*, **26**, 461–486.

Lecocq, G., Poitou, D., Hernandez, I., Duchaine, F., Riber, E., and Cuenot, B. 2014. A methodology for soot prediction including thermal radiation in complex industrial burners. *Flow Turbul. Combust.*, **92**(4), 947–970.

Lesieur, M., Métais, O., and Comte, P. 2005. *Large-Eddy Simulations of Turbulence*. Cambridge University Press, Cambridge UK.

Lu, T., and Law, C. K. 2005.A directed relation graph method for mechanism reduction. *Proc. Combust. Inst.*, **30**(1), 1333–1341.

Magnussen, B. F. 1981. On the structure of turbulence and a generalized eddy dissipation concept for chemical reaction in turbulent flow. Presented at the 19th AIAA Aerospace Science Meeting, St. Louis, Missouri, January. 12–15.

Marincola, F. C., Ma, T., and Kempf, A. M. 2013. Large eddy simulations of the Darmstadt turbulent stratified flame series. *Proc. Combust. Inst.*, **34**(1), 1307–1315.

Marzouk, O., and Huckaby, E. D. 2010. A comparative study of eight finite-rate chemistry kinetics for CO/H2 combustion. *Appl. Comp. Fluid Mech*, **4**, 331–356.

Meredith, K. V., and Black, D. L. 2006. Automated global mechanism generation for use in CFD simulations. Presented at the 44th AIAA-Aerospace science meeting and Exhibit, Reno, Nevada, January 9–12.

modeFRONTIER. 2015. Available at: http://www.modefrontier.com.

Moin, P. 2002. Advances in large eddy simulation methodology for complex flows. *Int. J. Heat Fluid Flow*, **23**(6), 710–720.

Nambully, S., Domingo, P., Moureau, V., and Vervisch, L. 2014a. A filtered-laminar-flame PDF sub-grid scale closure for LES of premixed turbulent flames. Part I: Formalism and application to a bluff-body burner with differential diffusion. *Combust. Flame*, **161**(7), 1756–1774.

Nambully, S., Domingo, P., Moureau, V., and Vervisch, L. 2014b. A filtered-laminar-flame PDF sub-grid scale closure for LES of premixed turbulent flames. Part II: Application to a stratified bluff-body burner. *Combust. Flame*, **161**(7), 1775–1791.

Nguyen, P.-D., Vervisch, L., Subramanian, V., and Domingo, P. 2010. Multidimensional flamelet-generated manifolds for partially premixed combustion. *Combust. Flame*, **157**(1), 43–61.

Nicoud, F., and Ducros, F. 1999. Subgrid-scale stress modelling based on the square of the velocity gradient tensor. *Flow Turbul. Combust.*, **62**, 183–200.

Niu, Y.-S., Vervisch, L, and Tao, P.D. 2013. An optimization-based approach to detailed chemistry tabulation: Automated progress variables definition. *Combust. Flame*, **160**(4), 776–785.

Novosselov, I.V, and Malte, P.C. 2008. Development and application of an eight-step global mechanism for CFD and CRN simulation of lean-premixed combustors. *J. Eng. Gas Turbine Power*, **130**(2), 021502.

O'Rourke, P.J., and Bracco, F.V. 1979. Two scaling transformation for the numerical computation of multidimensional unsteady laminar flames. *J. Comput. Phys.*, **33**(2):185–203.

Peters, N. 1985. Numerical and asymptotic analysis of systematically reduced reaction schemes for hydrocarbon flames. In G. Roland, L. Bernard, and T. Roger, (Eds.) *Numerical Simulation of Combustion Phenomena*, pp. 90–109. Springer Berlin Heidelberg, ISBN 978-3540-16073-1.

Peters, N. 2000. *Turbulent Combustion*, Cambridge University Press, Cambridge, UK.

Pitsch, H. 2006. Large eddy simulation of turbulent combustion. *Ann. Rev. Fluid Mech.*, **38**, 453–482.

Poinsot, T., and Veynante, D. 2005. *Theoretical and Numerical Combustion*, R. T. Edwards, Inc., Philadelphia.

Polifke, W., Geng, W., and Döbbeling, K. 1998. Optimization of rate coefficients for simplified reaction mechanisms with genetic algorithms. *Combust. Flame*, **113**(1–2), 119–134.

Proch, F. and Kempf, A. M. 2014. Numerical analysis of the Cambridge stratified flame series using artificial thickened flame LES with tabulated premixed flame chemistry. *Combust. Flame*, **161**(10): 2627–2646.

Prufert, U., Hartl, S., Hunger, F., Messig, D., Eiermann, M., and Hasse, C. 2015. A constrained control approach for the automated choice of an optimal progress variable for chemistry tabulation. *Flow Turbul. Combust.*, **94**(3): 593–617.

Razali, N.M., and Geraghty, J. 2011. Genetic algorithm performance with different selection straggles in solving TSP. In *Proceedings of the World Congress on Engineering*, vol. II, London. WCE.

Sadasivuni, S.K., Bulat, G., Sanderson V., and Swaminathan, N. 2012. Numerical application of scalar dissipation rate combustion model to Siemens DLE combustors. Presented at the ASME Turbo Expo, Copenhagen, Denmark, June 11–15.

Sagaut, P. 2001. *Large Eddy Simulation for Incompressible Flows: An Introduction*, 2nd eds., Springer-Verlag, Berlin Heidelberg.

Sikalo, N., Hasemann, O., Schulz, C., Kempf, A., and Wlokas, I. 2013. A genetic algorithm-based method for the automatic reduction of reaction mechanisms. *Int. J. Chem. Kinet.*, **46**(1), 41–59.

Slavinskaya, N., and Unkhoff, M.B. 2008. Reduced reaction mechanisms for methane and syngas combustion in gas turbines. *J. Eng. Gas Turbines Power*, **130**(2), 021504.

Smith, G.P., Golden, D.M., Frenklach, M., Moriarty, N.W., Eiteneer, B., Goldenberg, M., Bowman, C.T., Hanson, R.K., Song, S., Gardiner, W.C. Lissianski, V.V., and Qin, Z. 1999. Technical report. Available at: http://www.me.berkeley.edu/gri-mech/.

Srinivasan, S., Ranjan, R., and Menon, S. 2015. Flame dynamics during combustion instability in a high-pressure, shear-coaxial injector combustor. *Flow Turbul. Combust.*, **94**(1), 237–262.

Stopper, U., Aigner, M., Ax, H., Meier, W., Sadanandan, R., Stohr, M., and Bonaldo, A. 2010. PIV, 2D-LIF and 1D-Raman measurements of flow field, compostion and temperature in premixed gas turbine flames. *Exp. Therm. Fluid Sci.*, **34**(3), 396–403.

Stopper, U., Meier, W., Sadanandan, R., Stöhr, M., Aigner, M., and Bulat, G. 2013. Experimental study of industrial gas turbine flames including quantification of pressure influence on flow field, fuel/air premixing and flame shape. *Combust. Flame*, **160**(10), 2103–2118.

Subramanian, V., Domingo, P., and Vervisch, L. 2010. Large-eddy simulation of forced ignition of an annular bluff-body burner. *Combust. Flame*, **157**(3), 579–601.

Tham, Y.F., Bisetti, F., and Chen, J.Y. 2008. Development of a highly reduced mechanism for iso-octane HCCI combustion with targeted search algorithm. *J. Eng. Gas Turbine Power*, **130**(4), 042804.

Triantafyllidis, A., Mastorakos, E., and Eggels, R.L.G.M. 2009. Large eddy simulations of forced ignition of a non-premixed bluff-body methane flame with conditional moment closure. *combust. Flame*, **156**(12), 2328–2345.

Vanderbei, R.J., 2001. *Linear Programming: Foundations and Extensions*. Springer, New York. ISBN 0-7923-7342-1.

van Oijen, J.A., Lammers, F.A., and de Goey, L.P.H. 2001. Modeling of complex premixed burner systems by using flamelet-generated manifolds. *Combust. Flame*, **127**(3), 2124–2134.

Wang, G., Boileau, M., and Veynante, D. 2011. Implementation of a dynamic thickened flame model for large eddy simulations of turbulent premixed flames. *Combust. Flame*, **158**(11), 2199–2213.

Westbrook, C. K., and Dryer, F. L. 1984. Chemical kinetic modeling of hydrocarbon combustion. *Prog. Energy Combust. Sci.*, **10**(1), 1–57.